



**HAL**  
open science

# Bending Relaxation of H<sub>2</sub>O by Collision with Para - and Ortho -H<sub>2</sub>

Ricardo Manuel García-Vázquez, Alexandre Faure, Thierry Stoecklin

► **To cite this version:**

Ricardo Manuel García-Vázquez, Alexandre Faure, Thierry Stoecklin. Bending Relaxation of H<sub>2</sub>O by Collision with Para - and Ortho -H<sub>2</sub>. ChemPhysChem, 2023, 25 (2), 10.1002/cphc.202300698 . hal-04662060

**HAL Id: hal-04662060**

**<https://cnrs.hal.science/hal-04662060>**

Submitted on 26 Jul 2024

**HAL** is a multi-disciplinary open access archive for the deposit and dissemination of scientific research documents, whether they are published or not. The documents may come from teaching and research institutions in France or abroad, or from public or private research centers.

L'archive ouverte pluridisciplinaire **HAL**, est destinée au dépôt et à la diffusion de documents scientifiques de niveau recherche, publiés ou non, émanant des établissements d'enseignement et de recherche français ou étrangers, des laboratoires publics ou privés.



Distributed under a Creative Commons Attribution - NonCommercial - NoDerivatives 4.0 International License



# Bending Relaxation of H<sub>2</sub>O by Collision with *Para*- and *Ortho*-H<sub>2</sub>

Ricardo Manuel García-Vázquez,<sup>[a]</sup> Alexandre Faure,<sup>[b]</sup> and Thierry Stoecklin<sup>\*[a]</sup>

We extend our recent theoretical work on the bending relaxation of H<sub>2</sub>O in collisions with H<sub>2</sub> by including the three water modes of vibration coupled with rotation, as well as the rotation of H<sub>2</sub>. Our full quantum close-coupling method (excluding the H<sub>2</sub> vibration) is combined with a high-accuracy nine-dimensional potential energy surface. The collisions of *para*-H<sub>2</sub>O and *ortho*-H<sub>2</sub>O with the two spin modifications of H<sub>2</sub> are considered and compared for several initial states of H<sub>2</sub>O. The convergence of the results as a function of the size of the

rotational basis set of the two colliders is discussed. In particular, near-resonant energy transfer between H<sub>2</sub>O and H<sub>2</sub> is found to control the vibrational relaxation process, with a dominant contribution of transitions with  $\Delta j_2 = j_2^f - j_2^i = +2, +4$ ,  $j_2^i$  and  $j_2^f$  being respectively the H<sub>2</sub> initial and final rotational quantum numbers. Finally, the calculated value of the H<sub>2</sub>O bending relaxation rate coefficient at 295 K is found to be in excellent agreement with its experimental estimate.

## Introduction

Until very recently, the modeling of molecular excitation in the interstellar medium only took into account the rotation of the molecules detected, due to the cold temperatures (< 100 K) prevailing in interstellar clouds. However, some of the most abundant triatomic interstellar molecules, such as HCN<sup>[1]</sup> and C<sub>3</sub>,<sup>[2]</sup> have been detected in highly excited vibrational states in warmer environments, e.g. in star-forming regions and in the envelopes of giant stars. The large quantity of water present in the Earth's atmosphere made it very difficult to detect H<sub>2</sub>O in ro-vibrationally excited states but the construction of the Atacama Large Millimeter/submillimeter Array (ALMA) interferometer partially overcame these constraints and enabled the first measurements of water transitions into vibrationally excited states, up to  $(\nu_1, \nu_2, \nu_3) = (0, 1, 1)$ , as part of the Atomium project.<sup>[3]</sup> More recently, the launch of the James Webb Space Telescope (JWST) has not only freed us from the Earth's atmosphere, but has also widened the window of detection to vibrational wavelengths, with e.g. the very recent detection of water vapor in the terrestrial planet-forming region of a protoplanetary disk.<sup>[4]</sup>

Collisional rate coefficients of H<sub>2</sub> with water in vibrationally excited levels are then urgently needed by the astrochemists. On the theoretical side, the first quantum calculations dedicated

to collisions involving vibrationally excited polyatomic molecules were performed by Dagdigian and Alexander in 2013<sup>[5]</sup> for the umbrella modes of NH<sub>3</sub> colliding with He and by Loreau and Van der Avoud in 2015 for the umbrella modes of NH<sub>3</sub> in collisions with He.<sup>[6]</sup> We developed our own approach to treat the bending relaxation of a linear triatomic molecule colliding with an atom shortly after and applied it to the He-HCN,<sup>[7,8]</sup> He-C<sub>3</sub><sup>[9-11]</sup> and He-DCN<sup>[12]</sup> collisions. This method uses the internal coordinates Hamiltonian developed by Handy and Tennyson<sup>[13]</sup> restricted to its rigid bender form to compute the triatomic molecule ro-vibrational bound state energies and wave functions. We extended this approach recently to collisions involving an atom and a non linear symmetric triatomic molecule and applied it to the bending relaxation of H<sub>2</sub>O colliding with *para*-H<sub>2</sub>.<sup>[14]</sup> *para*-H<sub>2</sub> being treated as fictitious atom. In 2021 the team of Guo used a very similar approach to treat the vibrational relaxation of water, including the bending and stretching modes, in collisions with Cl<sup>[15]</sup> and Ar.<sup>[16]</sup> They used Radau coordinates instead of Bond length Bond angle coordinates to obtain the triatomic energies and wave functions.

For many years the only calculations available regarding the H<sub>2</sub> + H<sub>2</sub>O collision and taking into account the rotation of H<sub>2</sub> as well as the bending and rotation of H<sub>2</sub>O were the Quasi-Classical Trajectory (QCT) calculations performed by Faure *et al.*<sup>[17]</sup> using the full-dimensional (9D) potential energy surface (PES), fully described in Valiron *et al.*<sup>[18]</sup> The first quantum calculations of the bending relaxation of water by collisions with H<sub>2</sub> taking into account the rotation of H<sub>2</sub> were performed by Wiesenfeld in 2021.<sup>[19]</sup> These calculations however did not include yet the coupling between the bending and rotation of H<sub>2</sub>O. The object of the present study is then to extend our previous work on this system<sup>[14]</sup> by taking also into account both the rotation of H<sub>2</sub> and the two stretching modes of H<sub>2</sub>O. To this aim we use the same 9D PES developed by Valiron *et al.*<sup>[18]</sup> The paper is organised as follows: In section Method the main elements of the method are briefly reminded and the

[a] R. M. García-Vázquez, Dr. T. Stoecklin  
UMR5255-CNRS, Université de Bordeaux,  
351 cours de la libération, F-33405 Talence, France  
E-mail: thierry.stoecklin@u-bordeaux.fr

[b] Dr. A. Faure  
Univ. Grenoble Alpes, CNRS, IPAG,  
F-38000 Grenoble, France

© 2023 The Authors. ChemPhysChem published by Wiley-VCH GmbH. This is an open access article under the terms of the Creative Commons Attribution Non-Commercial NoDerivs License, which permits use and distribution in any medium, provided the original work is properly cited, the use is non-commercial and no modifications or adaptations are made.

modifications necessary to perform the dynamics calculations are discussed. In section Calculations and Results the results are presented and the bending relaxation rate coefficient is compared to the experimental data available. In section Conclusions a few conclusions are given.

## Method

The rigid rotor Close Coupling equations for the collisions of  $\text{H}_2 + \text{H}_2\text{O}$  were given long ago in detail by Phillips *et al.*<sup>[20]</sup> and we refer the interested reader to this paper. The extension of the theory to vibrating molecules is straightforward and only a brief account of the main steps of the calculations will be given in section Close Coupling Equations. The Schrödinger equation of the system is expressed in the  $(X', Y', Z')$  Space fixed frame which is obtained by a simple rotation of the inertial  $\text{H}_2\text{O}$   $(X, Y, Z)$  frame illustrated in Figure 1 where  $\vec{R}$  is the intermolecular vector between the centers of mass of  $\text{H}_2\text{O}$  and  $\text{H}_2$  and  $(R, \theta_R, \varphi_R)$  are its spherical coordinates in this frame where the relative interaction potential briefly described in the following section is also computed. As can be seen on this figure the water molecule is lying in the XOZ molecular plane while the  $C_2$  Z axis is bisecting the bending angle.

## Potential Energy Surface

We use an 8D restriction to non vibrating  $\text{H}_2$  of the 9D PES of Valiron *et al.*<sup>[18]</sup> which is expanded in the rigid rotor Green's angular basis set<sup>[20]</sup>

$$t_{p_1, p_2, p}^{q_1}(\theta_2, \varphi_2, \theta_R, \varphi_R) = \frac{a_{p_1, p_2, p}^{q_1}}{(1 + \delta_{q_1, r_1})} \sum_{r_1, r_2} \begin{pmatrix} p_1 & p_2 & p \\ r_1 & r_2 & r \end{pmatrix} \times \quad (1)$$

$$Y_{p_2}^{r_2}(\theta_2, \varphi_2) Y_p^{r_1}(\theta_R, \varphi_R) [\delta_{q_1, r_1} + (-1)^{(p_1 + q_1 + p_2 + p)} \delta_{-q_1, r_1}]$$

for each value of the  $\text{H}_2\text{O}$  Radau coordinates  $(R_1, R_2, \alpha)$  and the intermolecular distance  $R$ :

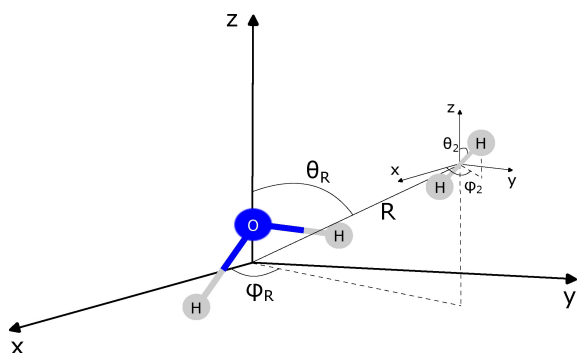


**Figure 1.** Coordinates used for the  $\text{H}_2\text{-H}_2\text{O}$  collision. The water molecule lies in the XOZ plane where O the  $\text{H}_2\text{O}$  center of mass and the Z axis is bisecting the bending angle.

$$V(R_1, R_2, \alpha, R, \theta_2, \varphi_2, \theta_R, \varphi_R) = \sum_{p_1, q_1, p_2, p} V_{p_1, p_2, p}^{q_1}(R_1, R_2, \alpha, R) t_{p_1, p_2, p}^{q_1}(\theta_2, \varphi_2, \theta_R, \varphi_R). \quad (2)$$

In Eq. (1), the normalization factor is:<sup>[18]</sup>

$$\alpha_{p_1, p_2, p}^{q_1} = [2(1 + \delta_{q_1, 0})^{-1} (2p_1 + 1)^{-1}]^{-1/2}. \quad (3)$$

## Calculations of the Ro-Vibrational Bound States of $\text{H}_2\text{O}$

Many papers have been devoted to the study of energy levels and spectra of the water molecule from the experimental and theoretical point of view. Very accurate results can be found, for example, in Ref. [21,22], and we encourage the people interested in the use of an extensive list of energy levels to refer to these papers. The first objective of this section is the determination of the  $\text{H}_2\text{O}$  rovibrational wave functions which will be used for performing the dynamics calculations. The second objective is to point out the main differences between our new approach and the one used in our previous work on the system<sup>[14]</sup> as well as with the widely used DVR3D method.<sup>[13]</sup>

In our previous work dedicated to the rigid bender inelastic collision of  $\text{H}_2\text{O}$  colliding with *para*- $\text{H}_2$ <sup>[14]</sup> we used bond length bond angle coordinates together with the Hamiltonian of Tennyson and Sutcliffe<sup>[21]</sup> to describe the internal motion of the water molecule. The rigid bender Hamiltonian equations were solved in the X bisector embedding frame and the solutions rotated in the X–Z plane by an angle of  $\frac{\pi}{2}$  in order to perform the dynamics.

In the present work, as we need to describe equally the stretching, bending and rotation of  $\text{H}_2\text{O}$ , we use instead Radau coordinates  $(R_1, R_2, \alpha)$  (see Figure 2) and the Z bisector

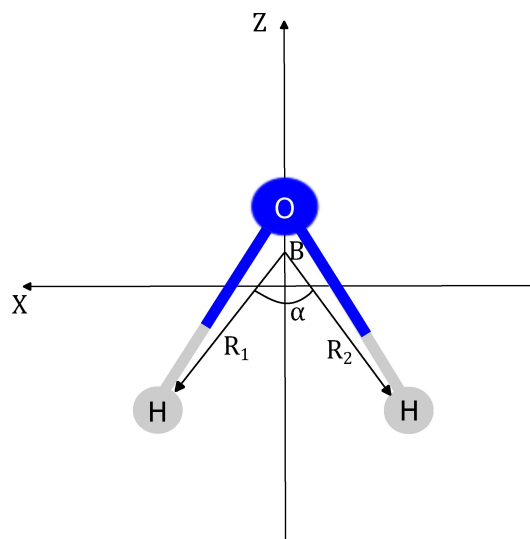


**Figure 2.** Coordinates used for the calculation of the  $\text{H}_2\text{O}$  bound states. B is the Radau canonical point of  $\text{H}_2\text{O}$ ,  $R_1$  and  $R_2$  are the modulus of the vectors that defines the position of the two hydrogen atoms with respect to the B point and  $\alpha$  is the angle between these two vectors.

embedding. This choice simplifies the hamiltonian by cancelling the radial cross derivatives that appears in the bond length bond angle Hamiltonian and also eliminating the need of the rotation step after diagonalization. It furthermore offers an excellent compromise of accuracy and computer time to calculate the H<sub>2</sub>O ro-vibrational bound states energies and wave functions as demonstrated by Tennyson.<sup>[13]</sup> In what follows we give the details of our implementation of the method for solving these equations as it differs in several respects from the approach used in the code DVR3D<sup>[13]</sup> like for example using Potential Optimised Discrete Variable Representation (PODVR).<sup>[15,22]</sup>

The H<sub>2</sub>O Hamiltonian takes the following form in Radau coordinates ( $R_1, R_2, \alpha$ ) and atomic units:<sup>[23]</sup>

$$\hat{H}_{ABC} = -\frac{1}{2\mu_1} \frac{\partial^2}{\partial R_1^2} - \frac{1}{2\mu_2} \frac{\partial^2}{\partial R_2^2} + \hat{T}_\alpha + \hat{T}_{vr} + V_{ABC}(R_1, R_2, \alpha) \quad (4)$$

where  $\hat{T}_\alpha$  and  $\hat{T}_{vr}$  are respectively the kinetic operators associated with the Radau angle  $\alpha$  and with the coupling between vibration and rotation as defined in Ref. [25] while the  $\mu_i$  are the reduced masses associated with the  $R_i$  coordinates.<sup>[13]</sup> The expression (4) is as usual re-written in terms of single radial coordinate hamiltonian of  $R_1$  and  $R_2$  as:

$$\hat{H}_{ABC} = \hat{h}_1(R_1) + \hat{h}_2(R_2) + \hat{T}_\alpha + \hat{T}_{vr} + \hat{V}_{res}(R_1, R_2, \alpha) \quad (5)$$

where  $\hat{h}_i, i = 1, 2$  are defined as:

$$\hat{h}_i(R_i) = -\frac{1}{2\mu_i} \frac{\partial^2}{\partial R_i^2} + \hat{V}_i(R_i) \quad (6)$$

These reference hamiltonians are similar to those used in Ref. [15] with the difference that we use the reduced masses  $\mu_1$  and  $\mu_2$  instead of the atomic masses  $m_A$  and  $m_C$ . The  $\hat{V}_i(R_i)$  and  $\hat{V}_{res}(R_1, R_2, \alpha)$  potentials are defined in the same way as in Ref. [15]:

$$\hat{V}_1(R_1) = \hat{V}_{ABC}(R_1, R_2^e, \alpha^e) \quad (7)$$

$$\hat{V}_2(R_2) = \hat{V}_{ABC}(R_1^e, R_2, \alpha^e) \quad (8)$$

$$\hat{V}_{res}(R_1, R_2, \alpha) = \hat{V}_{ABC}(R_1, R_2, \alpha) - \hat{V}_1(R_1) - \hat{V}_2(R_2) \quad (9)$$

where ( $R_1^e, R_2^e, \alpha^e$ ) are the values of the Radau coordinates for the equilibrium geometry of the ABC molecule.

For the sake of simplicity the H<sub>2</sub>O rotational angular momentum  $j_1$  as well as its space fixed Z axis projection  $m_{j_1}$  will be denoted only  $j$  and  $m_j$  in the present section. The general basis set describing both the vibration and rotation of the triatomic molecule is written:

$$|n_1 n_2 n j \bar{k} m_j, p\rangle = |n_1\rangle |n_2\rangle |n j \bar{k} m_j, p\rangle. \quad (10)$$

where  $|n j \bar{k} m_j, p\rangle$  is the symmetrized rovibrational basis set describing the bending and rotation part as defined by Sutcliffe and Tennyson<sup>[26]</sup> and also used in our previous work.<sup>[14]</sup>

$$|n j \bar{k} m_j, p\rangle = \frac{1}{\sqrt{2(1+\delta_{\bar{k},0})}} [ |n j \bar{k} m_j\rangle + (-1)^p |j n - \bar{k} m_j\rangle ] \quad (11)$$

with

$$|j n \bar{k} m_j\rangle = P_n^{\bar{k}}(\cos\alpha) |j \bar{k} m_j\rangle \quad (12)$$

where  $m_j$  and  $\bar{k}$  are the projections of the H<sub>2</sub>O rotational angular momentum  $j$  along the  $z'$  space fixed and  $z$  molecular fixed axis respectively.  $P_n^{\bar{k}}(\cos\alpha)$  is a generalized Legendre function while  $|j \bar{k} m_j\rangle$  is a symmetric top wave function.  $|n_1\rangle$  and  $|n_2\rangle$  are the eigenvectors of the radial reference Hamiltonians  $\hat{h}_i, i = 1, 2$  in a PODVR approach:<sup>[15,24]</sup>

$$\hat{h}_i |n_i\rangle = \epsilon_{n_i}^i |n_i\rangle, i = 1, 2. \quad (13)$$

We use a Gauss-Lanczos-Morse-DVR (GLM-DVR) basis<sup>[27]</sup> as a primitive basis for the PODVR, instead of the usual sine-DVR basis considered for example in Ref. [15] as it describes better the anharmonicity of the radial reference potentials. The resulting irregular radial grid gives a very good accuracy for a reduced number of points.

For A<sub>2</sub>B molecules one may furthermore take advantage of the permutation symmetry and use a symmetrized radial basis:

$$|n_1 n_2, q\rangle = N_{n_1, n_2} [ |n_1 n_2\rangle + (-1)^{q+\bar{k}} |n_2 n_1\rangle ] \quad (14)$$

with  $N_{n_1, n_2} = \frac{1}{\sqrt{2(1+\delta_{n_1, n_2})}}$ ,  $n_1 \geq n_2$  for  $q + \bar{k}$  even and  $n_1 > n_2$  for  $q + \bar{k}$  odd.<sup>[13]</sup> This expression, as discussed in Tennyson *et al.*,<sup>[13]</sup> presents the great advantage to allow selecting *ortho* and *para* symmetry blocks of A<sub>2</sub>B molecules by choosing a value of  $q$ . In the case of water  $q = 0$  and  $q = 1$  are respectively associated with the *para* and *ortho* symmetries.

From the matrix elements of the triatomic hamiltonian in the unsymmetrized basis set reported in Refs. [15,25] one can easily derive the non-zero matrix elements in the symmetrized basis:

$$\langle n_1 n_2 n j \bar{k} m_j, q, p | \hat{h}_1 + \hat{h}_2 | n'_1 n'_2 n' j \bar{k} m_j, q, p \rangle = 2N_{n_1, n_2} N_{n'_1, n'_2} (\epsilon_{n_1} + \epsilon_{n_2}) \left[ \delta_{n_1, n'_1} \delta_{n_2, n'_2} + (-1)^{q+\bar{k}} \delta_{n_1, n'_2} \delta_{n_2, n'_1} \right] \quad (15)$$

$$\langle n_1 n_2 n j \bar{k} m_j, q, p | \hat{T}_\alpha + \hat{T}_{vr} | n'_1 n'_2 n' j \bar{k} m_j, q, p \rangle = M_{n_1, n_2, n'_1, n'_2, q, \bar{k}} \times \left\{ \frac{1}{8} [j(j+1) - \bar{k}^2] \delta_{n, n'} \right. \\ \left. + n(n+1) \delta_{n, n'} + \frac{1}{4} [j(j+1) - 3\bar{k}^2] E_{n, n' \bar{k}} \right\} \quad (16)$$

$$\langle n_1 n_2 n_j \bar{k} m_j, q, p | \hat{T}_\alpha + \hat{T}_v | n'_1 n'_2 n'_j \bar{k} \pm 1 m_j, q, p \rangle = \frac{1}{4} (1 + \delta_{\bar{k},0})^{\frac{1}{2}} (1 + \delta_{\bar{k}\pm 1,0})^{\frac{1}{2}} \lambda_{j\bar{k}}^\pm R_{n_1, n_2, n_j, n_2, q, \bar{k}} \quad (17)$$

$$\times \left\{ (2\bar{k} + 1) (G_{n, n', \bar{k}} - D_{n, n', \bar{k}}) - 2\lambda_{n, \bar{k}}^\pm \delta_{n, n'} \right\}$$

$$\langle n_1 n_2 n_j \bar{k} m_j, q, p | \hat{T}_\alpha + \hat{T}_v | n'_1 n'_2 n'_j \bar{k} \pm 2 m_j, q, p \rangle = \frac{1}{16} (1 + \delta_{\bar{k},0})^{\frac{1}{2}} (1 + \delta_{\bar{k}\pm 2,0})^{\frac{1}{2}} \lambda_{j\bar{k}}^\pm \lambda_{j\bar{k}\pm 1}^\pm \times \quad (18)$$

$$M_{n_1, n_2, n_j, n_2, q, \bar{k}} \times (2F_{n, n', \bar{k}} - H_{n, n', \bar{k}})$$

with  $\lambda_{jm}^\pm = \sqrt{l(l+1) - m(m\pm 1)}$  and:

$$M_{n_1, n_2, n_j, n_2, q, \bar{k}} = 2N_{n_1, n_2} N_{n_j, n_2} \times \left[ A_{n_1, n_2, n_j, n_2} + (-1)^{q+\bar{k}} A_{n_1, n_2, n_j, n_j} \right], \quad (19)$$

$$R_{n_1, n_2, n_j, n_2, q, \bar{k}} = 2N_{n_1, n_2} N_{n_j, n_2} \times \left[ B_{n_1, n_2, n_j, n_2} + (-1)^{q+\bar{k}} B_{n_1, n_2, n_j, n_j} \right], \quad (20)$$

$$A_{n_1, n_2, n_j, n_2} = \langle n_1 n_2 | \frac{1}{2\mu_1 R_1^2} + \frac{1}{2\mu_2 R_2^2} | n_j, n_2 \rangle, \quad (21)$$

$$B_{n_1, n_2, n_j, n_2} = \langle n_1 n_2 | \frac{1}{2\mu_1 R_1^2} - \frac{1}{2\mu_2 R_2^2} | n_j, n_2 \rangle. \quad (22)$$

where the  $E_{n, n', \bar{k}}$ ,  $G_{n, n', \bar{k}}$ ,  $D_{n, n', \bar{k}}$ ,  $F_{n, n', \bar{k}}$  and  $H_{n, n', \bar{k}}$  are angular integrals defined in Ref. [25] which are computed using a Gauss-Legendre quadrature. For  $\bar{k} = \bar{k}' = 1$  there is an extra term in the symmetrized hamiltonian coming from the  $\bar{k} \pm 2, \bar{k}$  elements when  $\bar{k}' = -1$  and  $\bar{k} = 1$  in the unsymmetrized basis. This extra terms is defined as:

$$\langle n_1 n_2 n_j (\bar{k} = 1) m_j, q, p | \hat{T}_\alpha + \hat{T}_v | n'_1 n'_2 n'_j (\bar{k} = 1) m_j, q, p \rangle = \frac{(-1)^{j-p}}{16} j(j+1) M_{n_1, n_2, n_j, n_2, q, \bar{k}} \times (2F_{n, n', \bar{k}} - H_{n, n', \bar{k}}) \quad (23)$$

The symmetrised integrals over the potential take the following form:

$$\langle n_1 n_2 n_j \bar{k} m_j, q, p | V_{res}(R_1, R_2, \alpha) | n'_1 n'_2 n'_j \bar{k} m_j, q, p \rangle = 2N_{n_1, n_2} N_{n_j, n_2} \times \left[ \langle n_1 n_2 n_j \bar{k} m_j | V_{res}(R_1, R_2, \alpha) | n_1 n_2 n_j \bar{k} m_j \rangle \right. \quad (24)$$

$$\left. + (-1)^{q+\bar{k}} \langle n_1 n_2 n_j \bar{k} m_j | V_{res}(R_1, R_2, \alpha) | n_2 n_1 n_j \bar{k} m_j \rangle \right]$$

They are computed using a Gauss-Legendre quadrature for the integration over the Radau bending angle ( $\alpha$ ) and a GLM-PODVR quadrature over the radial Radau coordinates.

## Close Coupling Equations

We follow closely the approach detailed in the original paper of Phillips *et al.*<sup>[20]</sup> dedicated to the rigid rotor approach of the H<sub>2</sub> – H<sub>2</sub>O collisions where the reader can find the details of the derivation. We here only give their slightly modified form in order to refer to the three modes of vibration of the H<sub>2</sub>O molecule which can be coupled by the intermolecular potential. We do not include the H<sub>2</sub> vibration in our notation as it is neglected in the present approach ( $R_{HH} = 1.4a_0$ ). We will for rotation refer to the angular momenta  $\vec{j}_1$ ,  $\vec{j}_2$  and  $\vec{l}$  associated respectively with H<sub>2</sub>O, H<sub>2</sub> and their relative angular momentum while  $\vec{j}_{12} = \vec{j}_1 + \vec{j}_2$  and the  $\tau$  index allows distinguishing the H<sub>2</sub>O rotational states inside a given  $j_1$  multiplet. In order to further simplify the notations we will use the collective index ( $i$ ) to designate the set of quantum numbers ( $\nu_1 \nu_2 \nu_3 j_1 \tau j_2$ ) associated with a given internal state of the H<sub>2</sub> – H<sub>2</sub>O complex, where ( $\nu_1 \nu_2 \nu_3$ ) are the vibrational quantum numbers for, respectively, the symmetry stretching, the bending, and the antisymmetric stretching of H<sub>2</sub>O. The close-coupling equations for the radial part of the scattering wave function read:

$$\left\{ \frac{d^2}{dR^2} - \frac{l(l+1)}{R^2} + k_{(i),(j)}^2 \delta_{(i),(j)} \delta_{j_1 \tau j_2} \delta_{l l'} \right. \quad (25)$$

$$\left. - [U(R)]_{(i)j_1 \tau j_2 l; (j)j_1 \tau j_2 l'}^{JMP} \right\} \times G_{(i)j_1 \tau j_2 l; (j)j_1 \tau j_2 l'}^{JMP}(R) = 0$$

where  $G_{(i)j_1 \tau j_2 l; (j)j_1 \tau j_2 l'}^{JMP}(R)$  is the radial part of the H<sub>2</sub> – H<sub>2</sub>O scattering wave function,  $k_{(i)}^2 = 2\mu[E - \varepsilon_{(i)}]$  and

$$[U(R)]_{(i)j_1 \tau j_2 l; (j)j_1 \tau j_2 l'}^{JMP} = 2\mu \sum_{p_1 q_1 p_2 p} \langle (i)j_1 \tau JM | t_{p_1 p_2 p}^{q_1} | (j)j_1 \tau' JM \rangle \times \quad (26)$$

$$\int_0^\pi d\alpha \sin(\alpha) \int dR_1 \int dR_2 [F_{\nu_1 \nu_2 \nu_3}^{j_1 \tau}(R_1, R_2, \alpha) \times V_{p_1 p_2 p}^{q_1}(R_1, R_2, \alpha, R) \times F_{\nu_1' \nu_2' \nu_3'}^{j_1 \tau'}(R_1, R_2, \alpha)]$$

In this expression the  $F_{\nu_1 \nu_2 \nu_3}^{j_1 \tau}(R_1, R_2, \alpha)$  are the H<sub>2</sub>O wave functions calculated in the previous section while the  $\langle (i)j_1 \tau JM | t_{p_1 p_2 p}^{q_1} | (j)j_1 \tau' JM \rangle$  are the rigid rotor analytical angular matrix elements of the potential given in the paper of Phillips *et al.*<sup>[20]</sup>  $J$  and  $M$  are respectively the total angular momentum and its projection along the Z space fixed axis while  $P$  is the parity of the system. We furthermore replace the  $\varepsilon_{(i)}$  calculated in the previous section by their experimental values.

A new code called *Divitas* and including many of the ingredients of the *Newmat*<sup>[28]</sup> and *Didimat*<sup>[29]</sup> code was written in Bordeaux. It includes the calculations of the ro-vibrational states of H<sub>2</sub>O detailed in section Calculations of the Ro-Vibrational Bound States of H<sub>2</sub>O and solves the space fixed Close Coupling Eq. (25) using a log derivative propagator.<sup>[30]</sup> It was tested by reproducing the rigid rotor calculations performed in Grenoble using the *Molscat* code.<sup>[31]</sup>

## Calculations and Results

### H<sub>2</sub>O Bound States

We use the most recent POKAZATEL PES of water<sup>[22]</sup> to compute the energy levels of the water molecule for 8 values of the rotational state  $j_1 = 0 - 7$ . This PES which is the most accurate available was specifically designed to describe very excited ro-vibrational H<sub>2</sub>O states. Our basis set contains 4 GLM-PODVR functions for each  $R_1$  and  $R_2$  radial coordinates and 45 values of  $n$ . Angular integrals were computed using 50 Gauss-Legendre quadrature points while the radial integrals use a two dimensional  $R_1, R_2$  grid of 10 GLM-PODVR points for  $q + \bar{k}$  even and 6 points for  $q + \bar{k}$  odd due to the use of radial symmetrized basis.

The GLM-PODVR basis set is eigenfunction of the 1D reference hamiltonian  $\hat{h}_1$  (due to the symmetry of the water molecule  $\hat{h}_1$  and  $\hat{h}_2$  are identical) and is obtained using a 100 point 1D GLM-DVR spanning the  $[0.9, 4.5] a_0$  interval. A grid of 30 points is enough to achieve a convergence better than  $0.3 \text{ cm}^{-1}$  for all the calculated states and better than  $0.01 \text{ cm}^{-1}$  if we consider only the rotational states inside the  $(0, 0, 0)$ ,  $(0, 1, 0)$  and  $(0, 2, 0)$  vibrational states. The comparison with experiment shows the very good accuracy achieved in the present calculations. For all the 320 ro-vibrational states

computed in the present work, the maximum percentage error was 0.222% for *para* states and 0.218% for the *ortho* ones.

Very accurate H<sub>2</sub>O ro-vibrational bound state energies were reported by POKAZATEL<sup>[22]</sup>. These authors used the parametrised POKAZATEL PES<sup>[22]</sup> that was calculated from *ab initio* points and fitted to the experimental energy values with the help of the DVR3D package.<sup>[13]</sup> This semi empirical PES error leads to a very good accuracy of the bound state energies which is better than  $0.05 \text{ cm}^{-1}$  provided that the DVR3D method is used for the bound states calculations as it was used to perform the fit. As we do not use the DVR3D method, we compare our results with other non-semi-empirical values provided by the same authors using just an *ab initio* PES.<sup>[21]</sup> We present in Table 1 the results of this comparison and observe their excellent agreement. We furthermore can see that our most accurate results are obtained from the PES of Ref. [21] which is not semi empirical. We then conclude that the use of the *ab initio* + semi-empirical PES<sup>[22]</sup> leads to better results only if the DVR3D method which was used to perform the fit is also used to calculate the levels. A comparison with the rovibrational states recently computed by Yang *et al.*<sup>[32]</sup> using their *ab initio* PES is also presented in Table 2. The present approach appears to be more accurate by about a factor of ten.

**Table 1.** Comparison between theory and experiment of the 4 first excited vibrational energy levels of H<sub>2</sub>O ( $j = 0$ ) calculated using our approach and the POKAZATEL PES<sup>[22]</sup> (TW) or the PES reported in Ref. [21] (TW2). The errors reported in Ref. [21] (POL) using DVR3D<sup>[13]</sup> are reported in the last column. Units are  $\text{cm}^{-1}$ .

$(\nu_1, \nu_2, \nu_3)$	(EXP-TW)	(EXP-TW2)	(EXP-POL)
(0,1,0)	0.374	0.158	-0.310
(0,2,0)	0.727	0.484	-0.540
(1,0,0)	0.840	-0.242	-0.840
(0,0,1)	0.838	-0.039	-0.730

### Close-Coupling Calculations

As mentioned in section Close Coupling Equations the new code is an extension of the *Newmat* code version which was recently developed for treating the bending relaxation of H<sub>2</sub>O colliding with an atom.<sup>[14]</sup> It was then tested by reproducing calculations performed in recent work for the bending relaxation of H<sub>2</sub>O by collisions with He.<sup>[33]</sup> It was also tested by reproducing Molscat rigid rotor calculations for the H<sub>2</sub> + H<sub>2</sub>O collisions<sup>[34]</sup> using the experimental values of the H<sub>2</sub> rotational constants.<sup>[35]</sup> For all the calculations presented, three levels of

**Table 2.** Comparison of the experimental energy levels of *para*- and *ortho*-H<sub>2</sub>O (EXP) with the theoretical results reported in Yang *et al.*<sup>[32]</sup> (YA) and the ones obtained in this work (TW). The experimental values as well as the absolute errors are reported in  $\text{cm}^{-1}$ .

$(\nu_1, \nu_2, \nu_3)$	$J_{kac}$	EXP	(EXP-YA)	(EXP-TW)	$(\nu_1, \nu_2, \nu_3)$	$J_{kac}$	EXP	(EXP-YA)	(EXP-TW)
<i>para</i> -H <sub>2</sub> O					<i>ortho</i> -H <sub>2</sub> O				
(0,0,0)	0 <sub>00</sub>	0	0	0	(0,0,0)	1 <sub>01</sub>	23.794	0.094	-0.016
(0,1,0)	0 <sub>00</sub>	1594.746	-0.754	0.374	(0,1,0)	1 <sub>01</sub>	1618.557	-0.643	0.302
(0,2,0)	0 <sub>00</sub>	3151.630	-2.170	0.727	(0,2,0)	1 <sub>01</sub>	3175.441	-2.159	0.598
(1,0,0)	0 <sub>00</sub>	3657.053	9.253	0.840	(1,0,0)	1 <sub>01</sub>	3680.454	9.354	0.877
	1 <sub>11</sub>	3693.294	9.494	0.857		1 <sub>10</sub>	3698.491	9.491	0.957
	2 <sub>02</sub>	3725.942	9.442	0.920		2 <sub>12</sub>	3734.897	9.597	0.837
	2 <sub>11</sub>	3750.465	9.565	0.934		2 <sub>21</sub>	3788.694	10.094	1.079
	2 <sub>20</sub>	3789.969	10.069	0.882		3 <sub>03</sub>	3791.372	9.672	0.887
	3 <sub>13</sub>	3796.540	9.740	0.980		3 <sub>12</sub>	3827.393	9.793	1.134
	4 <sub>22</sub>	3966.559	10.359	0.911		3 <sub>21</sub>	3864.764	10.164	0.961
	5 <sub>33</sub>	4150.287	11.487	1.388		3 <sub>30</sub>	3935.345	11.045	1.014
(0,0,1)	1 <sub>01</sub>	3779.493	11.193	0.783	(0,0,1)	0 <sub>00</sub>	3755.928	11.128	0.838
	3 <sub>12</sub>	3926.862	11.662	1.218		3 <sub>22</sub>	3956.666	12.066	1.337

each  $H_2$  spin modification were necessary to converge the bending relaxation cross section. Rotational states of  $H_2O$  for  $j_1 = 0$  to 5 were included in the two bending states considered in the calculations. This choice of basis resulting from a compromise between computer time and accuracy allowed us to include the  $j = 5$  level of  $H_2$  which was neglected in previous calculations.<sup>[36]</sup> We checked that increasing the rotational basis set of  $H_2O$  up to  $j = 7$  only marginally affects the magnitude of the bending relaxation cross section for levels with  $j \leq 5$ . A Chebyshev grid of 18 bending angles and the same two dimensional  $R_1, R_2$  GLM-PODVR grid used before for the calculation of the wave functions of  $H_2O$  was used to calculate the vibrational part of the potential matrix elements while 20 closed channels were included for each collision energy in the  $0.1$ – $1000$   $cm^{-1}$  interval. This is corresponding to a maximum rotational energy of about  $4200$   $cm^{-1}$ , which is slightly higher than the  $3500$   $cm^{-1}$  used by Wiesenfeld.<sup>[19]</sup> Relative convergence of the bending relaxation cross section was tested as a function of the total angular momentum  $J$  for each collision energy to be better than  $10^{-6}$  leading to a maximum value of  $J = 65$  at  $1000$   $cm^{-1}$ , which is more than the double of the maximum value of  $J = 32$  used by Wiesenfeld.<sup>[36]</sup>

### Rotational Transitions Inside a Given Bending Level of $H_2O$

We compare in Figure 3 pure rotational transitions inside  $\nu_2 = 0$  and 1 and starting from the  $2_{20}$  level of  $H_2O$  in collision with *para*- $H_2$  ( $j_2 = 0$ ). The final state of  $H_2$  is ( $j_2 = 0$ ) for all the  $H_2O$  transitions represented. As can be seen on this figure the position of the resonances are about the same for the transitions considered inside the two different bending levels. The magnitudes are conversely seen to be slightly lower in the excited  $\nu_2 = 1$  level. This is not surprising as channels associated with excited levels of  $H_2$  (for example  $j_2 = 4 + H_2O(\nu_2 = 0, 5_{24})$ ) are open and interspersed between open  $\nu_2 = 1$  levels. This means that part of the scattering flux is directed to this open levels, lowering the magnitude of the cross sections obtained for the same transition inside the  $\nu_2 = 0$  bending level.

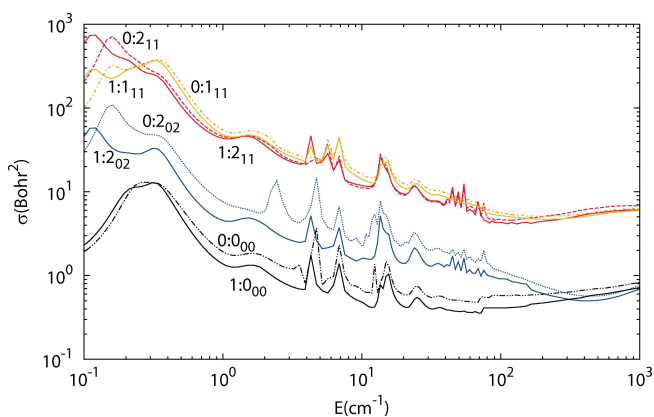


**Figure 3.** Comparison between rotationally inelastic state to state cross section for  $H_2O(\nu_2, 2_{20})$  colliding with *para*- $H_2$  ( $j = 0$ ) inside  $\nu_2 = 0$  and 1. The final  $H_2O$  ro-vibrational state is indicated on each curve. The solid and dashed line are respectively associated with transitions inside  $\nu_2 = 1$  and 0.

### Bending Relaxation Propensity Rules

#### Impact of the Initial and Final $H_2$ Rotational Basis

Figures 4, 5, 6, 7 show the bending relaxation cross sections for the four combinations of spin modifications of  $H_2$  and  $H_2O$  respectively *p*- $H_2 + p$ - $H_2O$ ; *p*- $H_2 + o$ - $H_2O$ ; *o*- $H_2 + p$ - $H_2O$  and *o*- $H_2 + o$ - $H_2O$ . On each of this figure the contributions of the three rotational levels of  $H_2$  considered in the calculations are reported as well as the total bending relaxation cross sections, again summed over the final states of water and  $H_2$ . If we consider first Figures 4 and 5 associated both with collisions of *p*- $H_2$  we see that the three  $j_2 = 0, 2$  and 4 final channels are open and give (except for the initial level *p*- $H_2$  ( $j_2 = 0$ ) +  $H_2O(1:0_{00})$ ) contributions in ascending order, the global bending relaxation cross section being always almost equal to the  $j_2 = 4$  contribution, except above  $\sim 200$ – $300$   $cm^{-1}$ . This is in contrast with rotational relaxation which favours the lowest  $\Delta j$ . As a matter of fact vibrational relaxation is conversely controlled by a near-resonant energy transfer mechanism which means that the largest contributions to the bending relaxation cross sections are provided by the internal levels of the complex which are the closest in energy with the initial level. Pure rotational transitions inside the excited bending level of  $H_2O$  give cross sections increasing with collision energy and up to five orders of magnitude larger than the bending relaxation cross sections, as illustrated in the upper left panel of Figure 4.

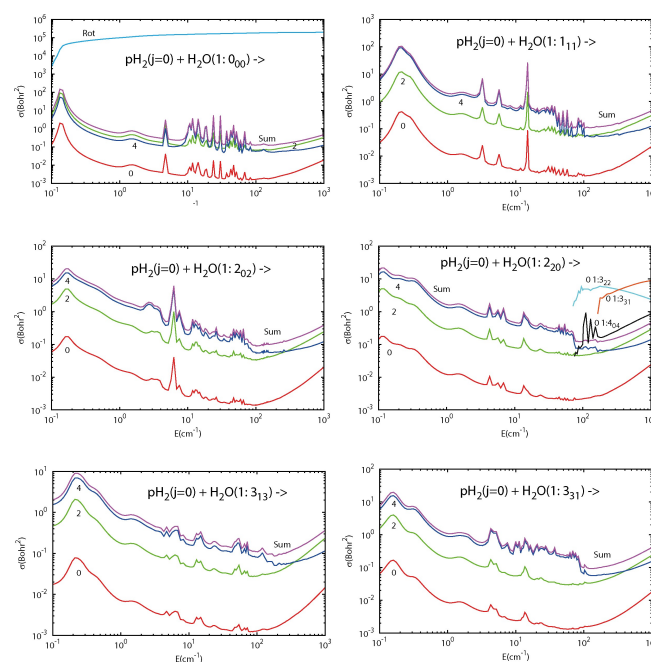


**Figure 4.** Comparison between the vibrational quenching cross section of *para*- $H_2O(\nu_2 = 1, j_{k_c})$  by collision with *para*- $H_2$  ( $j = 0$ ) for several initial levels of  $H_2O$  belonging to the  $\nu_2 = 1, j = 0, 1, 2$  and 3 manifolds. The curves 0, 2, 4 correspond to the final state of  $H_2$ . In the middle right panel the opening of excited state of  $H_2O$  is shown. The first reported quantum number on these curves is denoting the rotation of  $H_2$  while the others give the  $H_2O$  ro-vibrational state. In light blue (upper left panel) the summed rotationally inelastic cross section inside the initial  $\nu_2 = 1$  level is also represented for comparison.

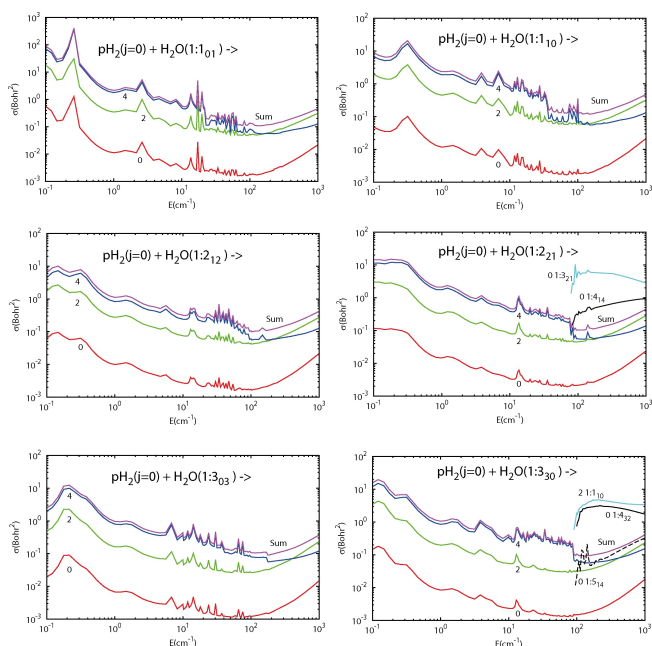


**Figure 5.** Comparison between the vibrational quenching cross section of *ortho*-H<sub>2</sub>O ( $\nu_2 = 1, j_{k_a k_c}$ ) by collision with *para*-H<sub>2</sub> ( $j = 0$ ) for several initial levels of H<sub>2</sub>O belonging to the  $\nu_2 = 1, j = 1, 2$  and 3 manifolds. In the lower and middle right panels the opening of excited states (higher in energy than the initial state) of H<sub>2</sub>O is also shown. The first reported quantum number on these curves is denoting the rotation of H<sub>2</sub> while the others give the H<sub>2</sub>O ro-vibrational state.

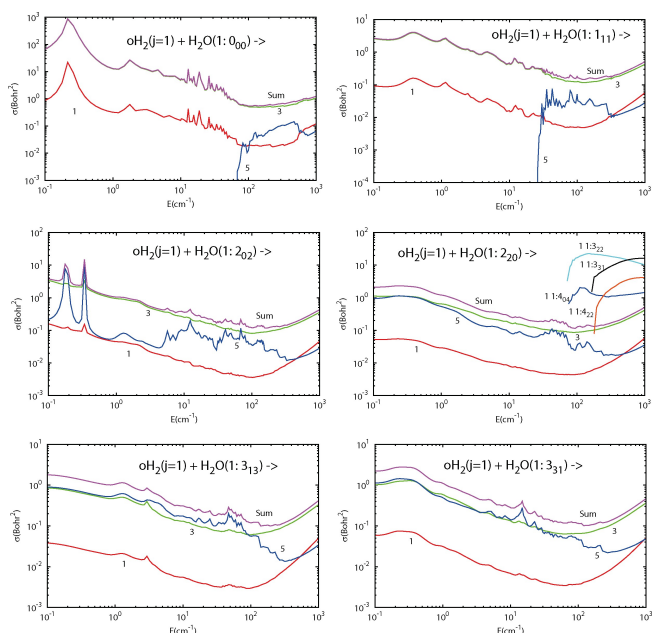


**Figure 6.** Comparison between the vibrational quenching cross section of *para*-H<sub>2</sub>O ( $\nu_2 = 1, j_{k_a k_c}$ ) by collision with *ortho*-H<sub>2</sub> ( $j = 1$ ) for several initial levels of H<sub>2</sub>O belonging to the  $\nu_2 = 1, j = 0, 1, 2$  and 3 manifolds. The curves 1, 3, 5 correspond to the final state of H<sub>2</sub>. In the middle right panel, state to state cross sections associated with the opening of a few excited levels (higher in energy than the initial level) of H<sub>2</sub>O are also represented. The first reported quantum number on these curves is denoting the rotation of H<sub>2</sub> while the others give the H<sub>2</sub>O ro-vibrational state.

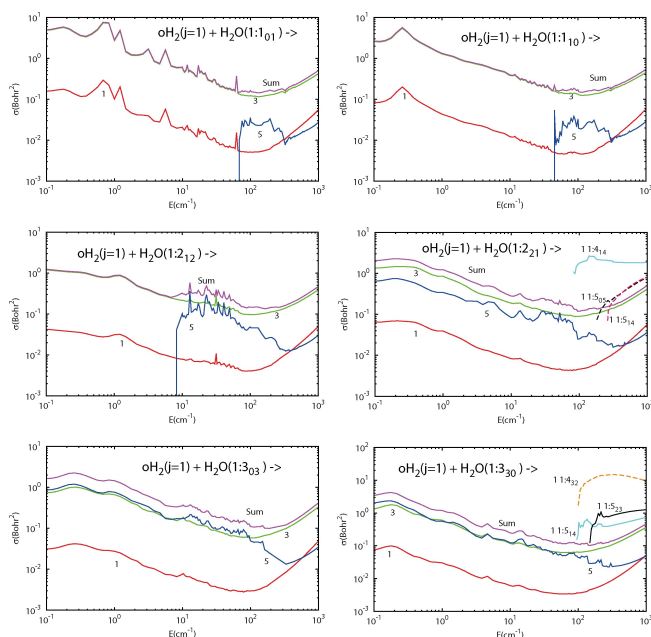


**Figure 7.** Comparison between the vibrational quenching cross section of *ortho*-H<sub>2</sub>O ( $\nu_2 = 1, j_{k_a k_c}$ ) by collision with *ortho*-H<sub>2</sub> ( $j = 1$ ) for several initial levels of H<sub>2</sub>O belonging to the  $\nu_2 = 1, j = 1, 2$  and 3 manifolds. In the middle and lower right panels the opening of excited states (higher in energy than the initial state) of H<sub>2</sub>O is also shown. The first reported quantum number on these curves is denoting the rotation of H<sub>2</sub> while the others give the H<sub>2</sub>O ro-vibrational state.

This results in the steps observed in the bending relaxation cross sections around  $70 \text{ cm}^{-1}$  associated with the opening of rotational levels inside the  $\nu_2 = 1$  excited bending level of H<sub>2</sub>O, as shown in the middle right panel of Figure 4 and in the right middle and lower panels of Figure 5 respectively for the opening of for example the *p*-H<sub>2</sub>( $j = 0$ ) + H<sub>2</sub>O( $\nu_2 = 1, 3_{22}$ ) and *p*-H<sub>2</sub>( $j = 0$ ) + H<sub>2</sub>O( $\nu_2 = 1, 3_{21}$ ) resulting in a decrease of the bending relaxation cross sections.

The strong dependence of the bending relaxation cross section as a function of the size of the H<sub>2</sub> rotational basis set included in the calculation explains why our first estimate of the bending relaxation cross section which considered only the  $j = 0$  state of H<sub>2</sub> was two orders of magnitude smaller than the experimental value at 300 K, as suggested in that work.<sup>[14]</sup>

If we now compare Figures 6 and 7 associated both with collisions of *o*-H<sub>2</sub> we see that the final level  $j_2 = 5$  is closed at low collision energy for many initial channels. This results in the main contribution to the bending relaxation cross section to be due to the  $j_2 = 3$  final level for almost all the initial levels represented. The contribution of the  $j_2 = 5$  final level is furthermore seen to exhibit many resonances as it is the closest in energy with the initial level and consequently the most sensitive to the opening of rotational levels inside the  $\nu_2 = 1$  level of H<sub>2</sub>O.

Impact of the initial H<sub>2</sub>O rotational basis

$j(\text{H}_2\text{O})$ -selected vibrational quenching rate coefficient of a given ( $\nu_2 = 1, j$ ) state of H<sub>2</sub>O are compared for the collisions with the two spin modifications of H<sub>2</sub> in their ground state in Figure 8. They were obtained by Boltzmann averaging all the asymmetric top multiplet contributions (i.e. for each  $j$ ) in the temperature range 0.5 – 500 K and by using the *ortho:para* statistical weight 3:1 for the water molecule. The global rate coefficient obtained by Boltzmann averaging the  $j = 0 - 3$  selected rates is also represented.

In the limit of low temperatures, the H<sub>2</sub>O ( $j = 0$ ) vibrational quenching rate is seen to be increasing as a function of temperature for the collisions with *o*-H<sub>2</sub> while it decreases as temperature increases for collisions with *p*-H<sub>2</sub>. We note that at higher temperatures (above 1500 K) which were not explored in the present approach, a rotational enhancement of the vibrational relaxation process was observed at the classical level for low  $j$  by Faure *et al.*<sup>[17]</sup> We indeed can already see for the collisions with both *p*- and *o*-H<sub>2</sub> that the  $j = 1$  state selected quenching rate becomes larger than the one of  $j = 0$  at higher temperature.

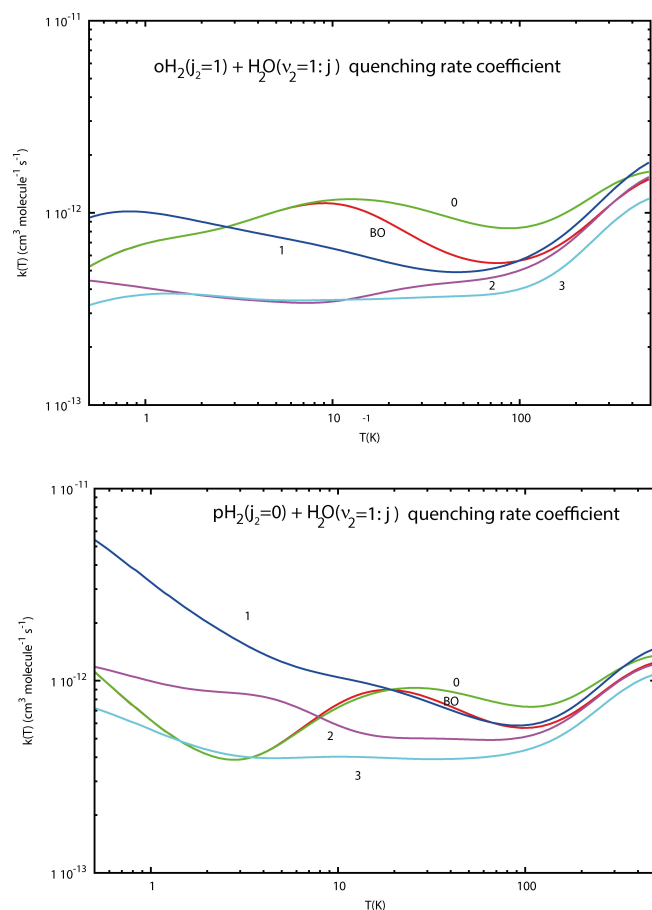


**Figure 8.** Comparison between the vibrational quenching rate coefficients of the ( $\nu_2 = 1, j = 0, 1, 2$  and  $3$ ) states of H<sub>2</sub>O by collision with H<sub>2</sub> and the Boltzmann averaged rate coefficient. The collisions with *para*-H<sub>2</sub> ( $j_2 = 0$ ) and with *ortho*-H<sub>2</sub> ( $j_2 = 1$ ) are respectively presented in the lower and upper panels.

We note that for astrophysical applications, the most extensive collisional dataset for H<sub>2</sub>O + H<sub>2</sub> is currently that of Faure and Josselin<sup>[38]</sup> which includes all H<sub>2</sub>O levels below 5000 cm<sup>-1</sup> and kinetic temperatures up to 5000 K. This dataset is based on literature data combined with a simple extrapolation procedure where rotation and vibration are fully decoupled. Our close-coupling calculations were limited here to water levels  $j = 0 - 5$  in the vibrational states (000) and (010) and kinetic temperatures lower than 500 K so that the present dataset as well as that of Wiesenfeld<sup>[36]</sup> are too small for actual astrophysical applications. Calculations will be extended to higher H<sub>2</sub>O ro-vibrational levels and higher kinetic temperatures in a future work and the new dataset will be made available in the BASECOL (<https://basecol.vamdc.eu/>) and EMAA databases (<https://emaa.osug.fr/>).

## Comparison with experiment

The contributions of *p*- and *o*-H<sub>2</sub> are Boltzmann averaged over  $j_2 = 0, 1, 2$  to obtain the global thermal rate coefficient which is presented in Figure 9, where it is compared to the only experimental data available at 295 K. A first interesting result appears on this figure as contribution of *o*-H<sub>2</sub> is seen to be negligible below 30 K, but slightly increases with temperature and becomes significant above 100 K. Our computed value at 295 K is  $1.18 \times 10^{-12}$  cm<sup>3</sup> molecule<sup>-1</sup> s<sup>-1</sup> in excellent agreement with the experimental value of  $(1.3 \pm 0.2) \times 10^{-12}$  cm<sup>3</sup> molecule<sup>-1</sup> s<sup>-1</sup>.

Interestingly, our value is about three times lower than the one obtained for *o*-H<sub>2</sub>O by Wiesenfeld<sup>[19]</sup> who used a simple direct product of a rigid rotor basis for the rotation and a normal mode function for the vibration. It is however difficult to compare the two kind of calculations which differ in several other aspects. The rotational basis sets both for H<sub>2</sub> and H<sub>2</sub>O are different and this author also performed calculations only for selected values of  $J$  and interpolated the cross sections for the missing values of  $J$ . In order to analyse more clearly the effect of

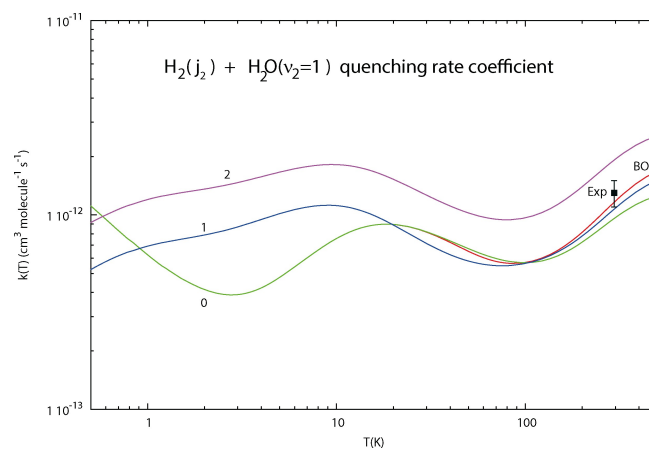


**Figure 9.** Comparison between the vibrational quenching rate coefficients of H<sub>2</sub>O ( $\nu_2 = 1$ ) by collision with the two spin modifications of H<sub>2</sub> and the global Boltzmann averaged rate coefficient. The only experimental value<sup>[37]</sup> available at 295 K is also reported.

the bending-rotation coupling we then performed new calculations presented in the following paragraph.

### Bending-Rotation Coupling

We investigate the effect of the coupling between bending and rotation by performing a new set of calculations neglecting this coupling by using for water a direct product of mono dimensional bending wave function and rigid asymmetric top rotational wave functions while keeping the experimental ordering of the H<sub>2</sub>O energies. As we are only interested, in the present study, in the two lowest bending levels of H<sub>2</sub>O the coupling with the two stretches can be safely neglected. This approach is very similar to the one used by Wiesenfeld<sup>[36]</sup> which consists in replacing  $I_{\nu_1\nu_2\nu_3}^{j_1j_2j_3}(R_1, R_2, \alpha)$  by  $I_{\nu_1\nu_2\nu_3}^{01}(R_1, R_2, \alpha)$  and  $I_{\nu_1\nu_2\nu_3}^{j_1j_2j_3}(R_1, R_2, \alpha)$  by  $I_{\nu_1\nu_2\nu_3}^{01}(R_1, R_2, \alpha)$  in Eq. (26).

We represented in the lower panel of Figure 10 the ratio of the present Close Coupling (denoted  $\sigma$ ) and approximate state to state cross section (denoted  $\sigma^{DP}$  for direct product) as a function of collision energy for the collisions of *p*-H<sub>2</sub> with H<sub>2</sub>O ( $\nu_2 = 1, 3_{31}$ ). As can be seen on this figure the ratio of the Close Coupling and approximate state to state cross sections is ranging from 0.4 to 2.2. The coupling is seen not surprisingly to be the strongest for collision energies corresponding to the

depth of the potential in the well and long-range regions. The strongest peaks which can be seen on this figure are associated with transitions towards the fundamental bending level: *p*-H<sub>2</sub>( $j_2 = 4$ ) + H<sub>2</sub>O( $\nu_2 = 0, 5_{24}$ ); *p*-H<sub>2</sub>( $j_2 = 2$ ) + H<sub>2</sub>O( $\nu_2 = 0, 5_{42}$ ); *p*-H<sub>2</sub>( $j_2 = 0$ ) + H<sub>2</sub>O( $\nu_2 = 0, 5_{24}$ ) and with  $\Delta j_2 = 2$ . Conversely the strongest bump at very low collision energy is associated with a pure rotational transition inside the excited H<sub>2</sub>O bending level towards *p*-H<sub>2</sub>( $j_2 = 0$ ) + H<sub>2</sub>O( $\nu_2 = 1, 3_{22}$ ).

If we now examine the ratio of the global bending relaxation cross section of H<sub>2</sub>O( $\nu_2 = 1, 3_{31}$ ) by collision with *p*-H<sub>2</sub> ( $j = 0$ ) represented in the upper panel of Figure 10 as a function of collision energy we find that the global error is divided by a factor two as the ratio is ranging from 0.7 to 1.4. The curve exhibits a succession of peaks located in the collision energy interval associated with the PES well, demonstrating clearly the resonant character of the coupling between bending and rotation.

### Conclusions

We presented the first calculations of the bending relaxation of H<sub>2</sub>O by collisions with the two spin modifications of H<sub>2</sub> when including exactly the coupling between H<sub>2</sub>O bending and rotation. The approach presented also considers the H<sub>2</sub>O stretching modes while only the two lowest bending levels were included in the present study. Our approach allowed us to obtain several important results. First, for collision energies associated with the region of the intermolecular potential well, roughly between 10 and 300 K, bending relaxation is controlled by a near-resonant energy transfer mechanism. Consequently, bending relaxation is larger towards the most excited final open rotational level  $j_2 = 4$  and decreases monotonously when  $j_2$  decreases for collisions with *p*-H<sub>2</sub>. In the case of collisions with *o*-H<sub>2</sub> it is the  $j_2 = 3$  final channel which is dominating as the  $j_2 = 5$  level is closed for several initial levels of the *o*-H<sub>2</sub> + H<sub>2</sub>O ( $\nu_2 = 1, jk_A k_C$ ) system. The Boltzmann weights make furthermore the contribution of the collisions with H<sub>2</sub> ( $j_2 = 1, 2$ ) negligible at low and moderate temperature. A very good approximation (10% error) of the global bending relaxation rate can be obtained by considering the process to be controlled by the collisions with *p*-H<sub>2</sub> for the whole interval of temperature of the present study (0.5 – 500K). Collisions with *o*-H<sub>2</sub> would not need in this case to be computed thus dividing computer time by more than a factor of two.

Our computed value of the global bending relaxation rate coefficient at 295 K is in excellent agreement with the experimental value. Future (ideally state-resolved) measurements over an extended range of temperatures will be useful to further test the predictions of the present calculations. We eventually investigated the decoupling between bending and rotation and found that the use of such an approximation leads to error ranging from 50% to 100% respectively for the bending relaxation and state to state cross sections.

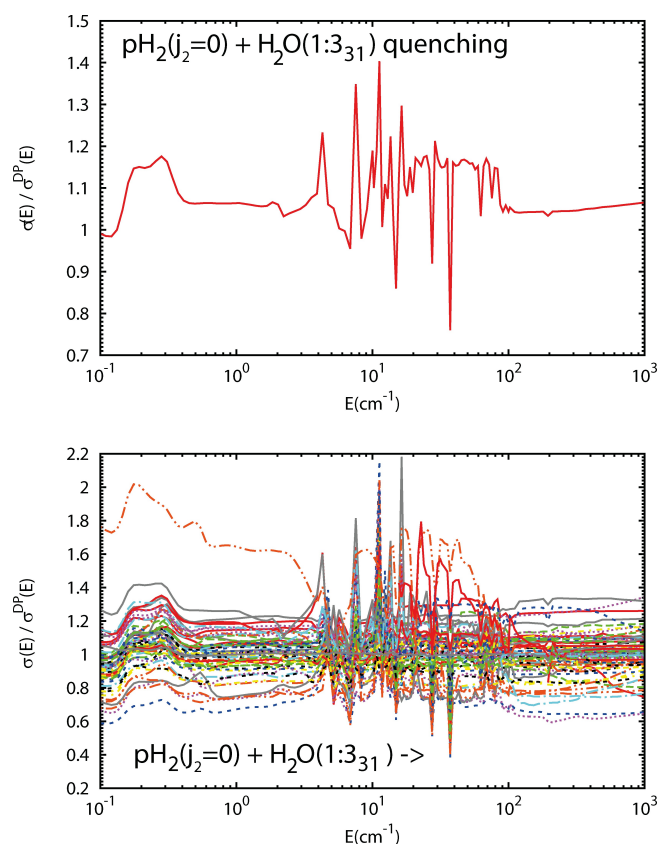


**Figure 10.** This figure shows the ratio of Close Coupling and direct product state to state cross sections as a function of collision energy for the collisions of *p*-H<sub>2</sub> with H<sub>2</sub>O ( $\nu_2 = 1, 3_{31}$ ).

## Acknowledgements

This work was supported by the french Agence Nationale de la Recherche (ANR-Waterstars), Contract No. ANR-20-CE31-0011 and by the ECOS-SUD project C22E02. Most of the computer time for this study was provided by the *Mésocentre de Calcul Intensif Aquitaine* computing facilities of *Université de Bordeaux and Université de Pau et des Pays de l'Adour*. Part of the computations were performed using the GRICAD infrastructure (<https://gricad.univ-grenoble-alpes.fr>), which is supported by Grenoble research communities.

## Conflict of Interests

There is no conflict of interest to report.

## Data Availability Statement

The data that support the findings of this study are available from the corresponding author upon reasonable request.

**Keywords:** Astrochemistry · Collisional Energy Transfer · Inelastic Dynamics · Propensity Rules · Quantum Chemistry

- [1] J. Cernicharo, M. M. Agúndez, C. Kahane, M. Guélin, J. R. Goicoechea, N. Marcelino, E. D. Beck, L. Decin, *Astron. Astrophys.* **2011**, 529, L3.
- [2] J. Cernicharo, J. R. Goicoechea, E. Caux, *Astrophys. J.* **2000**, 580, L199.
- [3] A. Baudry, K. T. Wong, S. Etoka, A. M. S. Richards, H. S. P. Müller, F. Herpin, T. Danilovich, M. D. Gray, S. Wallström, D. Gobrecht, T. Khouri, L. Decin, C. A. Gottlieb, K. M. Menten, W. Homan, T. J. Millar, M. Montargès, B. Pimpanuwat, J. M. C. Plane, P. Kervella, *Astron. Astrophys.* **2023**, 674, A125.
- [4] G. Perotti, V. Christiaens, T. Henning, B. Tabone, L. B. F. M. Waters, I. Kamp, G. Olofsson, S. L. Grant, D. Gasman, J. Bouwman, M. Samland, R. Franceschi, E. F. van Dishoeck, K. Schwarz, M. Güdel, P. O. Lagage, T. P. Ray, B. Vandenbussche, A. Abergel, O. Absil, A. M. Arabhavi, I. Argyriou, D. Barrado, A. Boccaletti, A. C. o Garatti, V. Geers, A. M. Glauser, K. Justannont, F. Lahuis, M. Mueller, C. Nehmé, E. Pantin, S. Scheithauer, C. Waelkens, R. Guadarrama, H. Jang, J. Kanwar, M. Morales-Calderón, N. Pawellek, D. Rodgers-Lee, J. Schreiber, L. Colina, T. R. Greve, G. Östlin, G. Wright, *Nature* **2023**, 620, 516.
- [5] Q. Ma, P. J. Dagdigan, M. H. Alexander, *J. Chem. Phys.* **2013**, 138, 104317.
- [6] J. Loreau, A. van der Avoird, *J. Chem. Phys.* **2015**, 143, 184303.
- [7] T. Stoecklin, O. Denis-Alpizar, P. Halvick, M.-L. Dubernet, *J. Chem. Phys.* **2013**, 139, 124317.
- [8] O. Denis-Alpizar, T. Stoecklin, P. Halvick, M.-L. Dubernet, *J. Chem. Phys.* **2013**, 139, 034304.
- [9] M. M. Al Mogren, O. Denis-Alpizar, D. B. Abdallah, T. Stoecklin, P. Halvick, M.-L. Senent, M. Hochlaf, *J. Chem. Phys.* **2014**, 141, 044308.
- [10] O. Denis-Alpizar, T. Stoecklin, P. Halvick, *J. Chem. Phys.* **2014**, 140, 084316.
- [11] T. Stoecklin, O. Denis-Alpizar, P. Halvick, *Mon. Not. R. Astron. Soc.* **2015**, 449, 3420.
- [12] O. Denis-Alpizar, T. Stoecklin, P. Halvick, *Mon. Not. R. Astron. Soc.* **2015**, 143, 114304.
- [13] J. Tennyson, M. A. Kostin, P. Barletta, G. J. Harris, O. L. Polyansky, J. Ramanlal, N. F. Zobov, *Comput. Phys. Commun.* **2004**, 163, 85.
- [14] T. Stoecklin, O. Denis-Alpizar, A. Clergerie, P. Halvick, A. Faure, Y. Scribano, *J. Phys. Chem. A* **2019**, 123, 5704, PMID: 31192600.
- [15] D. Yang, D. Xie, H. Guo, *J. Phys. Chem. A* **2021**, 125, 6864.
- [16] L. Liu, D. Yang, H. Guo, D. Xie, *J. Phys. Chem. A* **2023**, 127, 195, PMID: 36574615.
- [17] A. Faure, L. Wiesenfeld, M. Wernli, P. Valiron, *J. Chem. Phys.* **2005**, 123, 104309.
- [18] P. Valiron, M. Wernli, A. Faure, L. Wiesenfeld, C. Rist, S. Kedzuch, J. Noga, *J. Chem. Phys.* **2008**, 129, 134306.
- [19] L. Wiesenfeld, *J. Chem. Phys.* **2021**, 155, 071104.
- [20] T. R. Phillips, S. Maluendes, S. Green, *J. Chem. Phys.* **1995**, 102, 6024.
- [21] O. L. Polyansky, R. I. Ovsyannikov, A. A. Kyuberis, L. Lodi, J. Tennyson, N. F. Zobov, *J. Phys. Chem. A* **2013**, 117, 9633, PMID: 23517285.
- [22] O. L. Polyansky, A. A. Kyuberis, N. F. Zobov, J. Tennyson, S. N. Yurchenko, L. Lodi, *Mon. Not. R. Astron. Soc.* **2018**, 2608, 2597.
- [23] J. Tennyson, B. T. Sutcliffe, *Int. J. Quantum Chem.* **1992**, 42, 941.
- [24] J. Echave, D. C. Clary, *Chem. Phys. Lett.* **1992**, 190, 225.
- [25] X. G. Wang, T. Carrington, *J. Chem. Phys.* **2017**, 146, 104105.
- [26] B. T. Sutcliffe, J. Tennyson, *Mol. Phys.* **1986**, 58, 1053.
- [27] V. Szalay, *J. Chem. Phys.* **1993**, 99, 1978.
- [28] T. Stoecklin, A. Voronin, J. Rayez, *Phys. Rev. A* **2002**, 66, 042703.
- [29] A. Faure, P. Jankowski, T. Stoecklin, K. Szalewicz, *Sci. Rep.* **2016**, 6, 28449.
- [30] D. E. Manolopoulos, *J. Chem. Phys.* **1986**, 85, 6425.
- [31] J. M. Hutson, S. Green, MOLSCAT: MOlecular SCATtering v. 14, Astrophysics Source Code Library, record ascl:1206.004 **2012**.
- [32] D. Yang, L. Liu, D. Xie, H. Guo, *Phys. Chem. Chem. Phys.* **2022**, 24, 13542.
- [33] T. Stoecklin, L. D. Cabrera-González, O. Denis-Alpizar, D. Páez-Hernández, *J. Chem. Phys.* **2021**, 154, 144307.
- [34] F. Daniel, J. R. Goicoechea, J. Cernicharo, M.-L. Dubernet, A. Faure, *Astron. Astrophys.* **2012**, 547, A81.
- [35] K. P. Huber, G. Herzberg, *Constants of diatomic molecules*, Springer US, Boston, MA **1979**.
- [36] L. Wiesenfeld, *J. Chem. Phys.* **2022**, 157, 174304.
- [37] P. F. Zittel, D. E. Masturzo, *J. Chem. Phys.* **1991**, 95, 8005.
- [38] A. Faure, E. Josselin, *Astron. Astrophys.* **2008**, 492, 257.

Manuscript received: September 26, 2023  
 Revised manuscript received: November 21, 2023  
 Accepted manuscript online: November 21, 2023  
 Version of record online: December 15, 2023